

Magnetorheological elastomer base isolator for earthquake response mitigation on building structures: modeling and second-order sliding mode control

Yang Yu¹, Sayed Royel², Jianchun Li^{*1}, Yancheng Li^{**1} and Quang Ha²

¹*School of Civil and Environmental Engineering, University of Technology Sydney, Ultimo, NSW 2007, Australia*

²*School of Electrical Mechanical and Mechatronic Systems, University of Technology Sydney, Ultimo, NSW 2007, Australia*

(Received January 16, 2016, Revised April 29, 2016, Accepted June 20, 2016)

Abstract. Recently, magnetorheological elastomer (MRE) material and its devices have been developed and attracted a good deal of attention for their potentials in vibration control. Among them, a highly adaptive base isolator based on MRE was designed, fabricated and tested for real-time adaptive control of base isolated structures against a suite of earthquakes. To perfectly take advantage of this new device, an accurate and robust model should be built to characterize its nonlinearity and hysteresis for its application in structural control. This paper first proposes a novel hysteresis model, in which a nonlinear hyperbolic sine function spring is used to portray the strain stiffening phenomenon and a Voigt component is incorporated in parallel to describe the solid-material behaviours. Then the fruit fly optimization algorithm (FFOA) is employed for model parameter identification using testing data of shear force, displacement and velocity obtained from different loading conditions. The relationships between model parameters and applied current are also explored to obtain a current-dependent generalized model for the control application. Based on the proposed model of MRE base isolator, a second-order sliding mode controller is designed and applied to the device to provide a real-time feedback control of smart structures. The performance of the proposed technique is evaluated in simulation through utilizing a three-storey benchmark building model under four benchmark earthquake excitations. The results verify the effectiveness of the proposed current-dependent model and corresponding controller for semi-active control of MRE base isolator incorporated smart structures.

Keywords: magnetorheological elastomer (MRE) base isolator; earthquake mitigation; sliding mode control

1. Introduction

Today, one main challenge in structural engineering research is to find out an effective and reliable technique to protect the structures and their substances from damage and destruction

*Corresponding author, E-mail: jianchun.li@uts.edu.au

**Corresponding author, E-mail: yancheng.li@uts.edu.au

caused by external hazardous loadings such as strong winds, earthquake events, vibration shocks and destructive waves (Tavakoli *et al.* 2015, Hosseini and Farsangi 2012). Especially, seismic hazards in the past two decades all over the world have sufficiently proved the significance and necessity of alleviating the influence of such natural disasters on structures (Murase *et al.* 2013, Takewaki and Tsujimoto 2011). The concept of utilizing control system to deflect, offset or break up the energy caused by vibration is regarded as an ideal solution in this hot issue.

The control system is generally divided into passive, active, semiactive and hybrid according to required energy level as well as adopted device type (Spencer 2004, Spencer and Nagarajaiah 2003, Ha *et al.* 2013). Among these types, the semiactive control has obtained increasingly attractive attentions in structural vibration alleviation due to the benefits of low power requirement, mechanical simplicity and controllable force capacity. Recently, magnetorheological elastomer (MRE)-based and magnetorheological fluid (MRF)-based devices have been extensively developed and used as semiactive control devices in the application of vibration reduction (Behrooz *et al.* 2014b, Yang *et al.* 2014, Yu *et al.* 2015a, Mei *et al.* 2013). MRE is mainly made up of magnetic particles, which can form a chain aggregate structure under magnetic field conditions (Yu *et al.* 2016). This unique characteristic makes MRE controllable and flexible so that it is able to undergo the large deformations in compression, tension and shear mode (Li *et al.* 2010, Ha *et al.* 2015). Besides, compared with MRF, MRE employs the silicon rubber as the carrier of magnetic particles, tackling the particle setting and fluid sealing problems, and thus acquiring more engineering applications than MRF (Feng *et al.* 2015). So far, a large number of MRE-based devices have been developed to satisfy different vibration control application. Du *et al.* (2011) designed a novel MRE isolator for the seat vibration control in vehicles. Ginder *et al.* (1999) developed an adjustable automotive bushing for vibration suppression of rotational and translational shifts of the wheels. In the application of civil engineering, Li *et al.* (2013) designed and tested a novel adaptive laminated MRE base isolator with 25 soft layers. The results of testing on a shake table demonstrate that the device can provide the considerable adjustable increments of both shear force and effective stiffness up to 1470% and 1630% of values at the passive state, respectively. Due to these features, the design of smart base isolation systems with MRE base isolator for seismic protection of buildings and bridges becomes possible and feasible.

Although the MRE-based devices have proved their potentials in vibration control, the major difficulty for the actual practice is to characterize the nonlinear and hysteretic responses of the device under sudden exoteric loadings. A rheological model was first proposed by Li *et al.* (2010) to portray the behaviour of MRE, which contains a stiffness component connected with a three-parameter rubber material model. Eem *et al.* (2012) designed a dynamic model composed of a Maxwell model in parallel with the Ramberg-Osgood model to depict the viscoelastic and nonlinear feature of the MRE material. A novel rheological model was developed considering all property conditions of MRE including magnetic field-energized feature, viscoelasticity of material and interface slide between particles and the matrix (Chen and Jerrams 2011). In the respect of MRE-based device modeling, Yang *et al.* (2013) adopted the classical Bouc-Wen model to model the adaptive MRE base isolator and gave the explanation on the relationships between model parameters and the shape of device responses. Behrooz *et al.* (2014a) combined a three-component solid model with the Bouc-Wen element for hysteresis modeling of variable stiffness and damping isolator (VSDI). Li *et al.* (2015) proposed a novel phenomenal model by adding a revised Maxwell model to the standard three-parameter model for describing the strain stiffening behaviour related to the MRE base isolator. Besides, the improved LuGre model and improved Dahl model are also explored for such an objective (Li *et al.* 2014, Yu *et al.* 2015b).

Except for highly nonlinear responses of the device caused by force-displacement hysteresis, limited shear force caused by applied current input constraint also poses a tough problem for MRE base isolators applied to structural vibration control. Concerning this issue, considerable studies have been carried out to design nonlinear controllers which are suitable and effective for vibration alleviation, and feasible for full scale implementation in engineering structures. Several control algorithms have been recently developed, including ON-OFF control (Jansen and Dyke 2000), linear quadratic regulator (LQR) control (Agrawal and Yang 1999), frequency control (Gu *et al.* 2015), Lyapunov-based control (Ha *et al.* 2008), etc. In these methods, the control signals are acquired and switched between 0 and maximum current rather than directly from the errors between forces. As a result, the optimal capacity of the designed controller will not be guaranteed. Furthermore, the process of energy dispersion and shift from magnetization hysteresis will result in heat which will reduce the shear force and material properties of MRE base isolator. Therefore, the increase of temperature caused by elastomer dispersion will influence the control performance through supplying currents. In view of this point, this paper intends to present a direct control of applied current level to the MRE base isolators combined with the protected structures.

In order to realize the field-controlled scheme for MRE base isolator installed with a building structure, a reliable and robust model should be developed to illustrate the nonlinearity with traceable relationships between model parameters and control signals. In this work, the unique responses of MRE base isolator is first analysed through a large quantity of experimental testing under various loading conditions. Then in accordance with the captured force-displacement/velocity responses, a novel hyperbolic hysteresis model is proposed based on the classic Bouc-Wen model, in which a hyperbolic sine function spring is employed to substitute for the Bouc-Wen element to describe the nonlinear and hysteretic responses of the device. The main benefit of this modification is to avoid the differential equations in the traditional MRE models, which makes the parameters easy to be identified. Model identification is considered as solving a minimization optimization problem and is realized using newly developed fruit fly optimization algorithm (FFOA). Furthermore, in order to adapt to various loading frequencies, a generalized current-dependent model is obtained by setting up the relationships between model parameters and applied magnetic fields. Finally, based on the proposed model, a second-order sliding mode controller is designed and its performance is evaluated in simulation of a three-storey building model equipped with two field-controlled MRE base isolators, subjected to four benchmark earthquakes: EI-Centro, Kobe, Hachinohe and Northridge. The results show that both inter-storey shift and acceleration are minimized therefore verifying the capacity of the proposed method in vibration control in civil structures.

2. Design and experimental testing of MRE base isolator

2.1 MRE base isolator design

An adaptive base isolator based on MRE was designed by Li *et al.* (2013) according to the laminated structure of rubber bearing, in which the traditional rubber component is replaced by thin MRE and steel plates so that the shear modulus of the device is able to be varied according to external energized magnetic fields. Fig. 1 shows the diagrammatical figure and real photo of adaptive MRE base isolator. In this design, 25 layers of soft MRE sheets with 120 mm diameter and 1 mm thickness are employed with 26 layers of steel sheets with the same diameter and

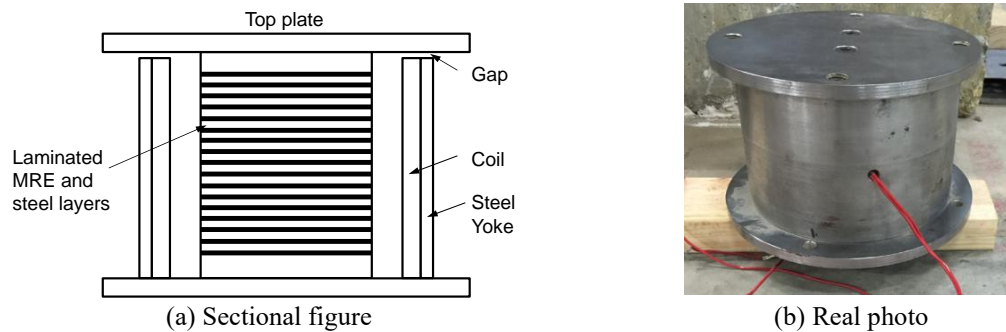


Fig. 1 Adaptive MRE base isolator (Li *et al.* 2013)

thickness. The steel sheets are used to provide the isolator with load-carrying capacity in the vertical direction, i.e., weight for the structure. For the base isolation system, the vibration control performance is mostly dependent on the lateral stiffness of the device $k=G_s \cdot A/h_t$, where G_s is the shear modulus of elasticity of MRE material, A is the cross-section area of the MRE layers and h_t is the thickness of the MRE layers. To ensure the best vibration isolation performance, the lateral stiffness should be carefully calculated and selected. Moreover, a solenoid, made of nonmagnetic support and electromagnetic coil, is deployed outside of the laminated bearing component to produce the constant magnetic field after supplied with DC current. The maximal permissible lateral displacement of the MRE base isolator is 15 mm. Thus without the applied current, the vertical loading support ability of the device can reach as high as 50 kg. And this value will increase with the ascending applied current and descending lateral displacement.

2.2 Experimental setup of MRE base isolator

In order to assess the capacity of the adaptive MRE base isolator, enormous experimental tests are undertaken using a shake table, which is utilized to produce the lateral loading to the isolator. Fig. 2 shows experimental setup for device performance testing. It is clearly seen that the device installed above the table shifts with the movement of the shake table. In addition, the system also has the load cell, the displacement sensor and DC power supply that are used to measure the shear force and displacement of the device, and provide the uniform magnetic field to the device, respectively. In the test, a large range of excitations with different loading frequencies, amplitudes and applied magnetic fields are selected to drive the isolator. In this work, three types of driven frequencies of 1 Hz, 2 Hz and 4 Hz and three amplitudes of 2 mm, 4 mm and 8 mm are chosen together with four applied current levels of 0A, 1A, 2A and 3A corresponding to different magnetic fields. To assure that the base isolator is tested in the steady condition, more than three cycles of responses (shear force and displacement) are captured for each excitation case. The sampling frequency is set as 256 Hz. To guarantee the stable capacity of the isolator, over 10 cycles of responses are captured for every loading condition. Moreover, each test is independently repeated five times to guarantee the consistency and accuracy of the result. After obtaining the displacement responses, the velocity responses can be calculated using finite-difference approximation method.

2.3 Testing results of MRE base isolator

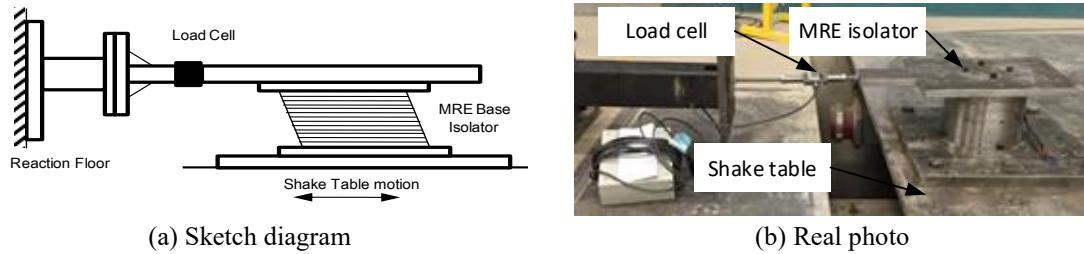


Fig. 2 Experimental setup

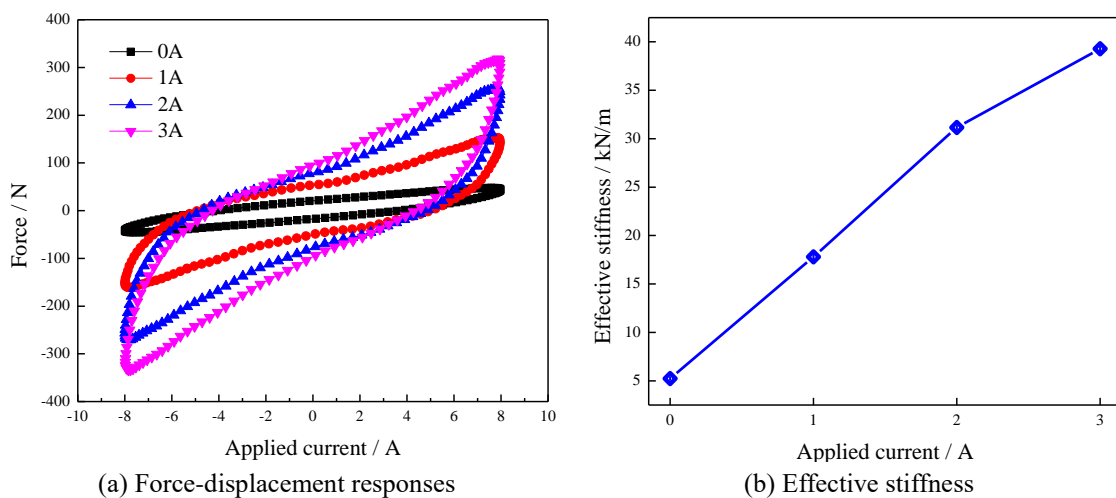


Fig. 3 Testing results of MRE isolator under 2 Hz frequency harmonic excitation with 8 mm amplitude

Fig. 3(a) presents the dynamic force-displacement responses when the device is driven by 2 Hz frequency sinusoidal excitation with 8 mm amplitude for all current levels ranging from 0A to 3A. According to this figure, an obvious increment of shear force with the applied magnetic field is observed. It also can be seen that the effective stiffness of the device, denoted as the slope of the response loop, displays a significant increase with the adding current. Fig. 3(b) shows the effective stiffness values of the device corresponding to different applied currents. The result proves that the device has a perfect linear relationship between effective stiffness and supplying current, which is beneficial to its practical control application.

3. Modeling of MRE base isolator

3.1 Classical MRE model

Few models have been reported to characterise the nonlinear and hysteretic responses of MRE isolators. Among them, the most commonly used model is the Bouc-Wen model (Yang *et al.* 2013). Bouc-Wen Model is composed of a linear spring, a viscous dashpot and a hysteretic component. This classical model is able to be represented by a force equation together with a related hysteresis variable y , shown as:

$$F = kx + c\dot{x} + \alpha y + F_0 \quad (1)$$

$$\dot{y} = \delta\dot{x} - \beta\dot{x}|y|^n - \gamma y|\dot{x}||y|^{n-1} \quad (2)$$

where k and c are stiffness and damping coefficients; α , β , δ , n and γ denote non-dimensional parameters of Bouc-Wen model ; y denotes the hysteresis variable; F_0 is the force offset. Note that the model indicates a conventional rubber bearing when the value of α equals to 0. Bouc-Wen model has been widely used in different engineering applications to characterise various hysteresis responses. Nevertheless, because of the addition of internal dynamics in relation to intermediate variable y of the device state, unexpected singularity may happen in the process of model identification.

3.2 Hyperbolic hysteresis model

Unlike other complex MRE models with differential equations, this paper proposes a relatively simple mathematical model to capture the nonlinear and hysteretic force-displacement responses of the device. A component-wise added method is applied which includes a viscos dashpot component, a linear spring and a strain stiffening element. The configuration of the proposed model is shown in Fig. 4.

In terms of mathematical expressions, the model utilizes a hyperbolic sine function spring to portray the phenomenon of stiffening hardening with the increasing current, and two linear functions to depict the viscos-elastic feature. The detailed presentation of the proposed model is shown as:

$$F = c_0\dot{x} + k_0x + \alpha z + F_0 \quad (3)$$

$$z = \frac{1 - e^{-2\beta x}}{2e^{-\beta x}} \quad (4)$$

where c_0 and k_0 denote the viscous and stiffness parameters, respectively; α denotes the scale coefficient to control the tendency of strain stiffening; β is the parameter to trim the hysteresis loop; F_0 denotes the force offset of the device and its value can be obtained by calculating the mean value of shear force in one sampling cycle.

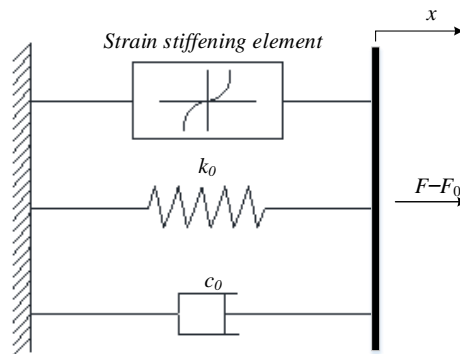


Fig. 4 Structure of hyperbolic hysteresis model

Compared with the Bouc-Wen model, the proposed hyperbolic hysteresis model has fewer model parameters to be identified. In addition, the proposed model has much simpler mathematical expression to demonstrate the hysteresis component than Bouc-Wen model, because there is no any highly nonlinear differential equation in the expression of the proposed model. It is generally known that the numerical integration methods such as Euler method or Runge Kutta method are employed to solve the differential equation in the Bouc-Wen model. However, these methods belong to the recursive algorithms, which may bring the iteration errors during the calculation process and result in more calculation time meanwhile. As a consequence, the proposed model should have higher accuracy, at least in theory, which is beneficial to the controller development.

3.3 Model identification

After the construction of MRE base isolator model, the following task is to identify the model parameters according to the captured force-displacement and force-velocity responses of each loading case. Because this model is highly nonlinear in which the parameters are difficult to search by trials, the process of the parameter identification is considered as solving a minimization optimization problem. The key issue of the optimization problem is the selection of the fitness function, which has a significant impact on the final recognition results. In this work, the root mean square (RMS) error between the experimental data and predictions from the proposed model in a sampling cycle is employed as the fitness for parameter identification, as shown in the following expression

$$Obj(S) = \sqrt{\frac{1}{N} \sum_{i=1}^N \left[F_i^{\text{exp}} - (c_0 \dot{x}_i + k_0 x_i + \alpha \cdot \frac{1 - e^{-2\beta x_i}}{2e^{-\beta x_i}} + F_0) \right]^2} \quad (5)$$

where $S=[c_0, k_0, \alpha, \beta]$ is the model parameter set to be identified; N is the total number of the experimental data in one sampling cycle; x_i , \dot{x}_i and F_i^{exp} denote the collected displacement, velocity and shear force of the device at i th sampling time point, respectively. If the value of $Obj(S)$ approximates to zero, the corresponding result S is treated as the optimal solution of the problem. In conclusion, the optimization problem can be formulated as the following expression with several constraint conditions

$$\min Obj(S) \quad s.t. \quad c_0 > 0, k_0 > 0, \alpha > 0, \beta > 0 \quad (6)$$

In the next step, the fruit fly optimization algorithm (FFOA), based on interactive evolutionary computation method simulated by the food search behaviour of fruit fly swarm, is adopted to deal with above optimization problem. Due to the superiority of smell and vision organs, the FFOA can reach the global optimum very quickly and has a better recognition performance over other commonly used swarm algorithms (Pan 2012, 2013, 2014). The procedure of FFOA to identify the model of MRE base isolator can be composed of the following steps:

Step 1. Determine the optimization problem and algorithm parameters: the optimization problem has been proposed in Eq. (6) and algorithm parameters include population size N_{pop} and maximal iteration number N_{iter} .

Step 2. Initialize the position of fruit fly swarm (x_axis , y_axis).

Step 3. Randomly assign the orientation and scope for food search by the personal fruit fly based

on smell organ, expressed as

$$x_i = x_axis + random_value \tag{7}$$

$$y_i = y_axis + random_value \tag{8}$$

Step 4. Because the information on food source is unknown, the range between *i*th fly coordinate and the original point (0, 0) is calculated first, denoted as *dis_i*. Then calculate the reciprocal of *dis_i* as the model parameter set *S_i* to be identified according to the following equations

$$dis_i = \sqrt{x_i^2 + y_i^2} \tag{9}$$

$$S_i = 1 / dis_i \tag{10}$$

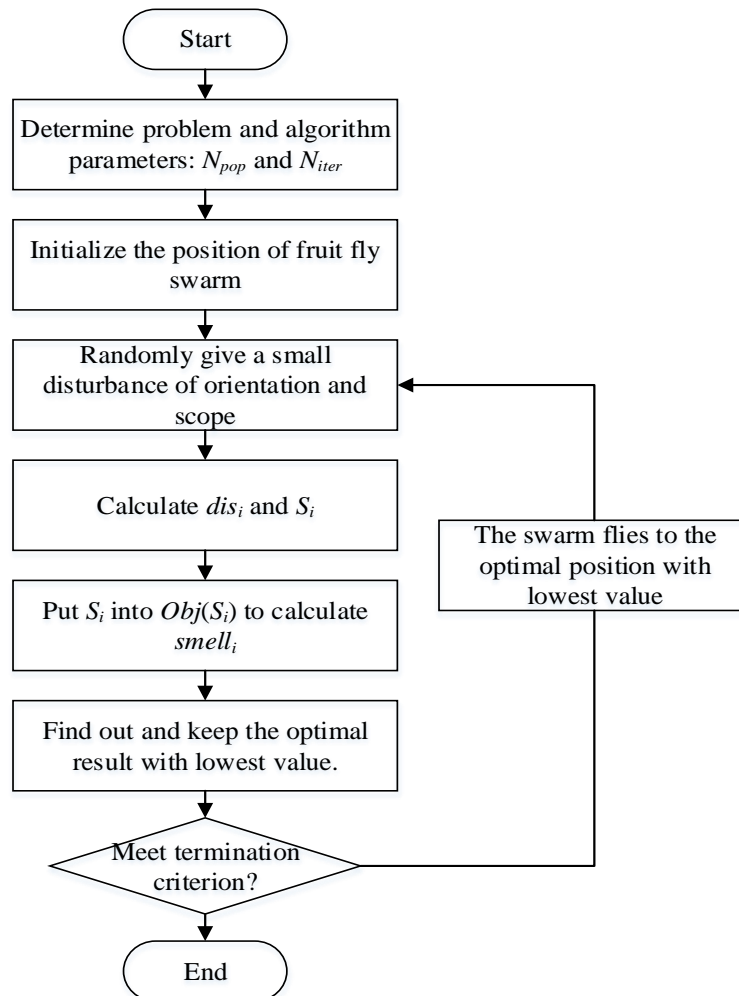


Fig. 5 Flow chart of FFOA to identify the hyperbolic hysteresis model

Step 5. Put the S_i into the fitness function $Obj(S_i)$ to calculate the smell concentration value ($smell_i$) of i th fruit fly. After obtaining all the smell concentration values of the swarm, the fruit fly with lowest smell concentration will be picked out and recorded in the system together with concentration value and corresponding coordinate

$$smell_i = Obj(S_i) \quad (11)$$

$$[optimal_smell, optimal_coordinate] = \min(smell_i) \quad (12)$$

Step 6. Record the optimal concentration value and corresponding coordinate. In the meantime, the overall swarm flies towards that optimal position.

Step 7. Repeat the Steps 2-5. If the calculated optimal concentration value is lower than the record, update the record through replacing it with the lower value. Otherwise, the record is unchanged. If the iteration number arrives at the maximal iteration, terminate the algorithm.

Fig. 5 illustrates the implementation of FFOA to calculate the parameter values of hyperbolic hysteresis model for MRE base isolator.

3.4 Modeling result and analysis

The implementation of FFOA to identify the novel hyperbolic hysteresis model is based on MATLAB v.2012b. The algorithm parameters are set as: $N_{pop}=50$ and $N_{iter}=300$. Fig. 6(a) describes one example of the flight path of fruit fly swarm for the parameter k_0 using FFOA when loading condition is 4 Hz frequency and 2 mm amplitude. The result demonstrates that this flying path of the fruit fly swarm is relatively steady without any big cornering. The whole swarm can directly fly towards the food source and quickly arrive at that position. Fig. 6(b) gives the convergence rate of the FFOA during the process of parameter identification. It is obviously seen that after 300 evolution iterations, the convergence rate is able to be obtained at the generation of 20 with the coordinate of (0.04401, 0.04306), and the corresponding parameter values of k_0 is 16.3818. The identification results for all loading conditions are given in Table 1.

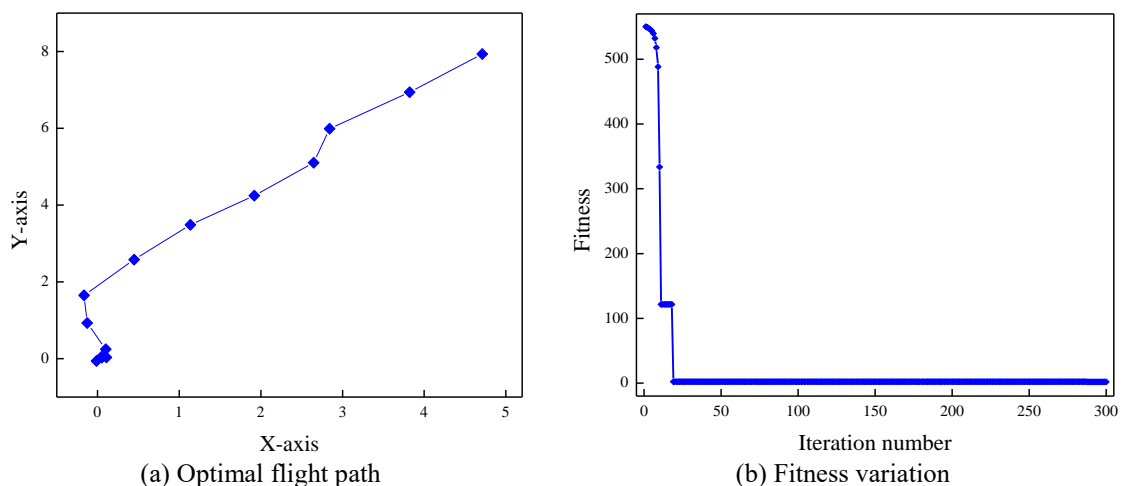


Fig. 6 Iteration process of parameter identification using FFOA

To demonstrate the effectiveness of the proposed model to describe the dynamic behaviours of the device, several comparative studies are conducted according to different loading conditions. The force-displacement responses of MRE base isolator under the 2 mm amplitude harmonic excitations and 1A current level are portrayed in Fig. 7(a) with predictions from the proposed model, while Fig. 7(b) gives the corresponding results of force-velocity responses. All the plots are drawn at three frequencies: 1 Hz, 2 Hz and 3Hz. It seems that three loops in the force-displacement responses overlap together, which directly demonstrates that the effective stiffness and the maximal shear force are independent of the exciting frequency. Unlike force-displacement responses, the loops in Fig. 7(b) have the obvious increments of nonlinear behaviours with the ascending frequency. According to the comparison results, the predictions from the proposed model perfectly agree with the experimental data under different frequency excitations.

Fig. 8(a) gives a group of comparison between predicted shear force and experimental data when loading the device with the 4 mm amplitude and 2 Hz frequency excitations. It is clearly

Table 1 Identification results for all the excitation conditions

Excitation		Parameter	Current level			
Frequency	Amplitude		0A	1A	2A	3A
1Hz	2 mm	k_0	4.0958	8.2243	13.1275	23.2931
		c_0	0.3537	2.1711	3.7312	4.2844
		α	14.7934	15.2078	26.4769	29.0083
		β	0.0622	0.8185	0.8817	0.8720
	4 mm	k_0	2.9999	7.8168	11.8441	19.0549
		c_0	0.3329	1.5603	2.5673	3.0085
		α	4.4035	12.5352	29.8296	23.7437
		β	0.3036	0.5271	0.4771	0.5692
	8 mm	k_0	2.3289	2.7041	1.4534	15.0109
		c_0	0.3062	1.1810	1.9238	2.2723
		α	14.4578	24.4383	22.1404	21.4932
		β	0.1292	0.2838	0.3889	0.3532
2Hz	2 mm	k_0	1.6444	18.4213	19.0493	27.9731
		c_0	0.2258	1.1576	1.9599	2.2876
		α	8.8277	23.8813	13.6024	24.0823
		β	0.4337	0.2823	1.1128	0.8684
	4 mm	k_0	2.6855	10.6519	14.9709	16.5911
		c_0	0.2127	0.8358	1.3552	1.5876
		α	11.8971	2.8526	17.5807	39.0569
		β	0.2063	0.8528	0.5698	0.4494
	8 mm	k_0	1.6707	9.8401	7.3621	13.9311
		c_0	0.1956	0.6410	1.0154	1.2077
		α	8.0351	1.8535	19.7717	19.0687
		β	0.2562	0.5285	0.3659	0.3742

Table 1 Continued

Excitation		Parameter	Current level			
Frequency	Amplitude		0A	1A	2A	3A
4Hz	2 mm	k_0	2.7132	16.3818	21.0926	39.5461
		c_0	0.1464	0.6477	1.0629	1.2206
		α	5.5715	3.7949	31.8038	2.8777
		β	0.6492	1.2273	0.6403	1.7722
	4 mm	k_0	5.3159	14.9349	17.1666	27.2481
		c_0	0.1384	0.4726	0.7372	0.8559
		α	5.0829	8.9217	6.6962	7.7418
		β	0.2159	0.3741	0.7907	0.7415
	8 mm	k_0	5.4541	5.1195	7.7478	12.4571
		c_0	0.1277	0.3664	0.5604	0.6561
		α	2.8212	8.6349	21.7603	30.5025
		β	0.1833	0.3952	0.3472	0.3169

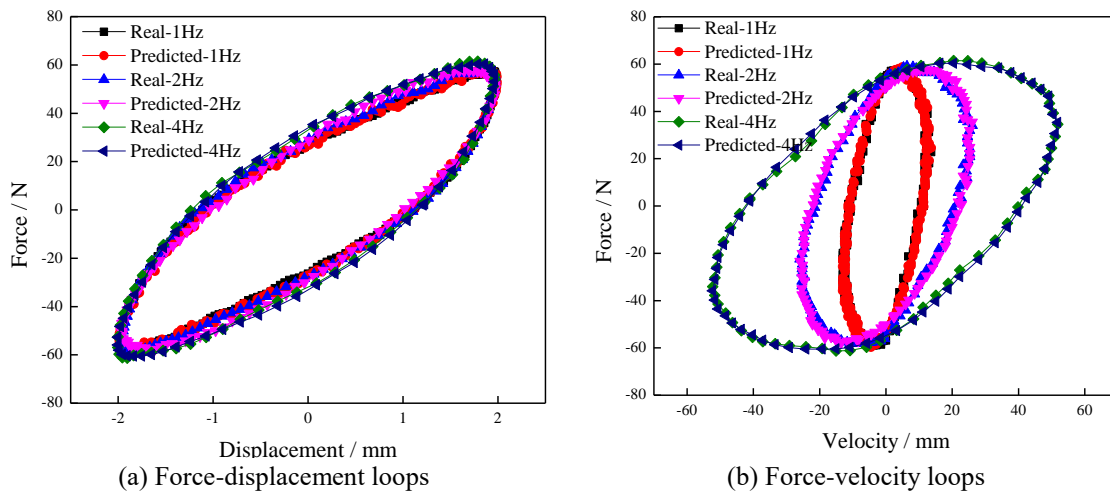
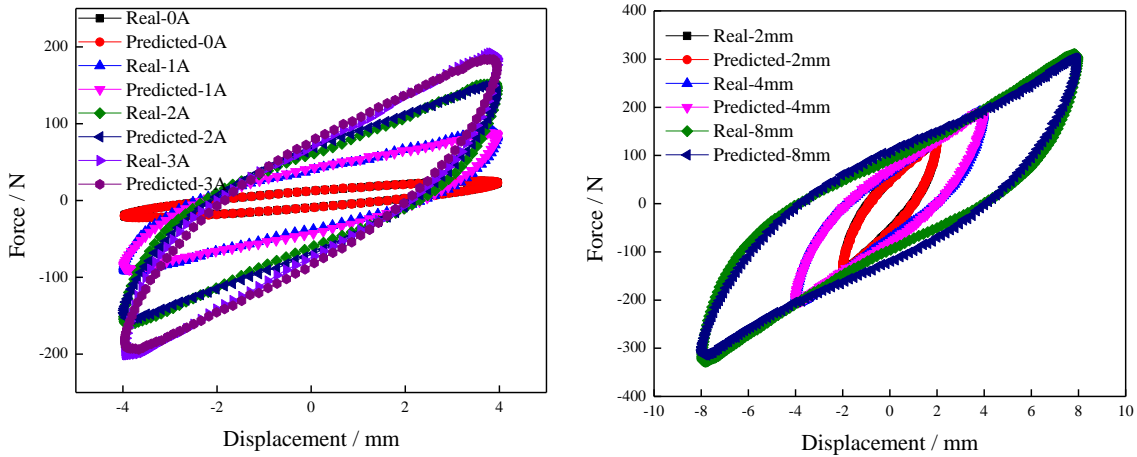


Fig. 7 Device responses under different loading frequencies (2mm-1A)

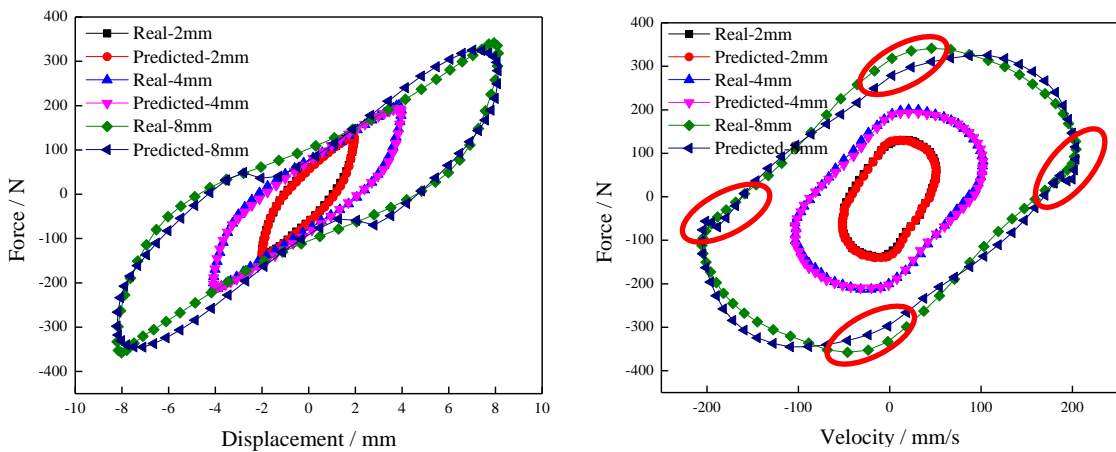
seen that the proposed model accurately illustrates the strain stiffening phenomenon of the device with the increasing current level. Fig. 8(b) shows the measured and predicted force-displacement loops acquired through loading the device with the 1 Hz frequency excitation and 3A applied current. In this case, the loading amplitude varies from 2 mm to 8 mm. An obvious feature to be noticed in this comparison is Mullins effect, in which the increasing excitation amplitude will result in the slight reduction of the effective stiffness. The results also demonstrate the capacity of the proposed model to capture this unique phenomenon of the device.

In order to further demonstrate the superiority of the proposed model over other existing MRE models, it is also compared with the classical Bouc-Wen model in terms of fitting curve, modelling error and running time. Similarly, the Bouc-Wen model is identified using the same



(a) Responses with different driven currents (b) Responses with different loading amplitudes

Fig. 8 Force-displacement responses between experimental results and model predictions



(a) Force-displacement loops (b) Force-velocity loops

Fig. 9 Comparison between experimental data and predictions from Bouc-Wen model

experimental data, objective function, optimization algorithm (FFOA) and algorithm parameters as the proposed hyperbolic hysteresis model. Fig. 9 gives the predicted responses from the Bouc-Wen model in the loading condition of the 4 Hz excitation with 3A current level. The comparison results seem that the Bouc-Wen model can provide the perfect agreements with the experimental data under the condition of small amplitudes (2 mm and 4 mm). However, when the loading amplitude grows to 8 mm, the Bouc-Wen model becomes less efficient (see Fig. 9(b)).

The RMS errors between shear forces acquired from the measurements and predictions from both Bouc-Wen and proposed models based on identified parameters are described in Fig. 10. When no current or low current level is applied to the isolator, two models have the similar RMS errors. Nevertheless, with the increase of the current level, the proposed model shows the higher identification accuracy than the Bouc-Wen model. Fig. 11 shows the running time of both models for the parameter identification under different loading conditions. For each case, the running time descends with the increasing frequency. This is mainly because the complete hysteresis loops

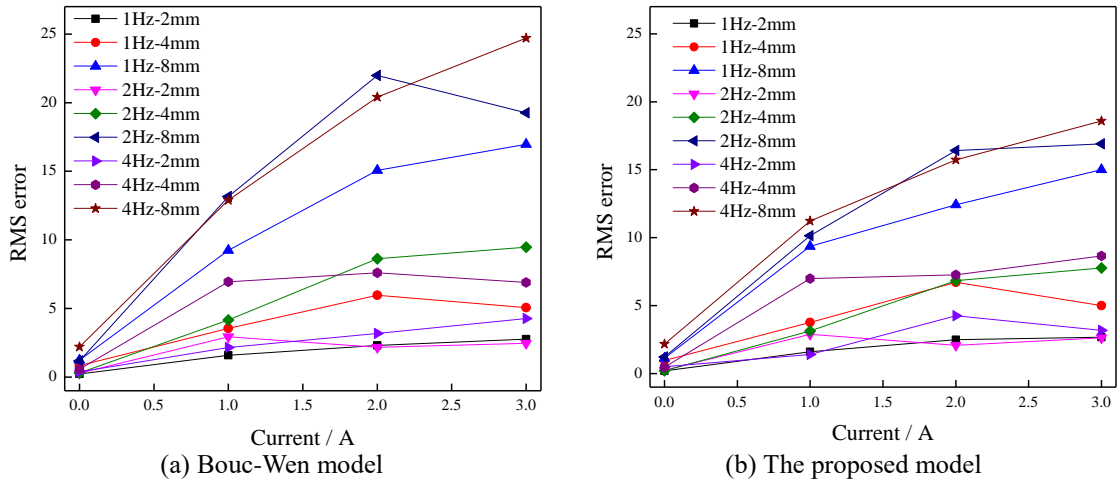


Fig. 10 RMS error of model identification using FFOA

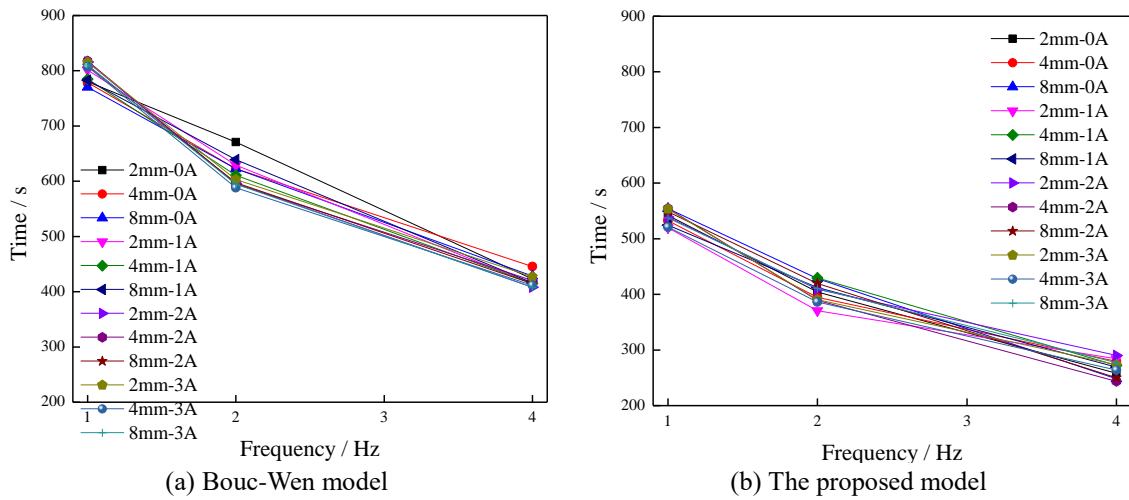


Fig. 11 Running time of model identification using FFOA

with different loading frequencies are made up of different numbers of sampling points. Besides, for the same loading condition, the Bouc-Wen model requires longer running time than the proposed model due to the high nonlinearity in the model together with more parameters to be identified. These results demonstrate that the proposed model is more accurate and efficient for modeling MRE base isolator.

3.5 Generalized field-dependent model

The parameters identified from the proposed model with different loading conditions are grouped in accordance with applied current levels. Then the values of these parameters are averaged in each current level, shown in Fig. 12. It is noticeable that the mean values of all the model parameters seem to have the almost linear relationships with the increasing currents.

Therefore, the 1st-order polynomial functions are selected to portray these relationships and the specific expressions are given as follows

$$k_0(i) = k_0^0 \cdot i + k_0^1 \tag{13}$$

$$c_0(i) = c_0^0 \cdot i + c_0^1 \tag{14}$$

$$\alpha(i) = \alpha^0 \cdot i + \alpha^1 \tag{15}$$

$$\beta(i) = \beta^0 \cdot i + \beta^1 \tag{16}$$

where $k_0^0, k_0^1, c_0^0, c_0^1, \alpha^0, \alpha^1, \beta^0$ and β^1 are constant coefficients of the polynomial functions, respectively; i denotes the applied current level. Least square (LS) method is used to calculate these coefficients and the corresponding results are given in Table 3. Finally, a generalized hyperbolic hysteresis model is built, the expression of which is given as follows

$$F = c_0(i)\dot{x} + k_0(i)x + \alpha(i) \cdot \frac{1 - e^{-2\beta(i)x}}{2e^{-\beta(i)x}} + F_0 \tag{17}$$

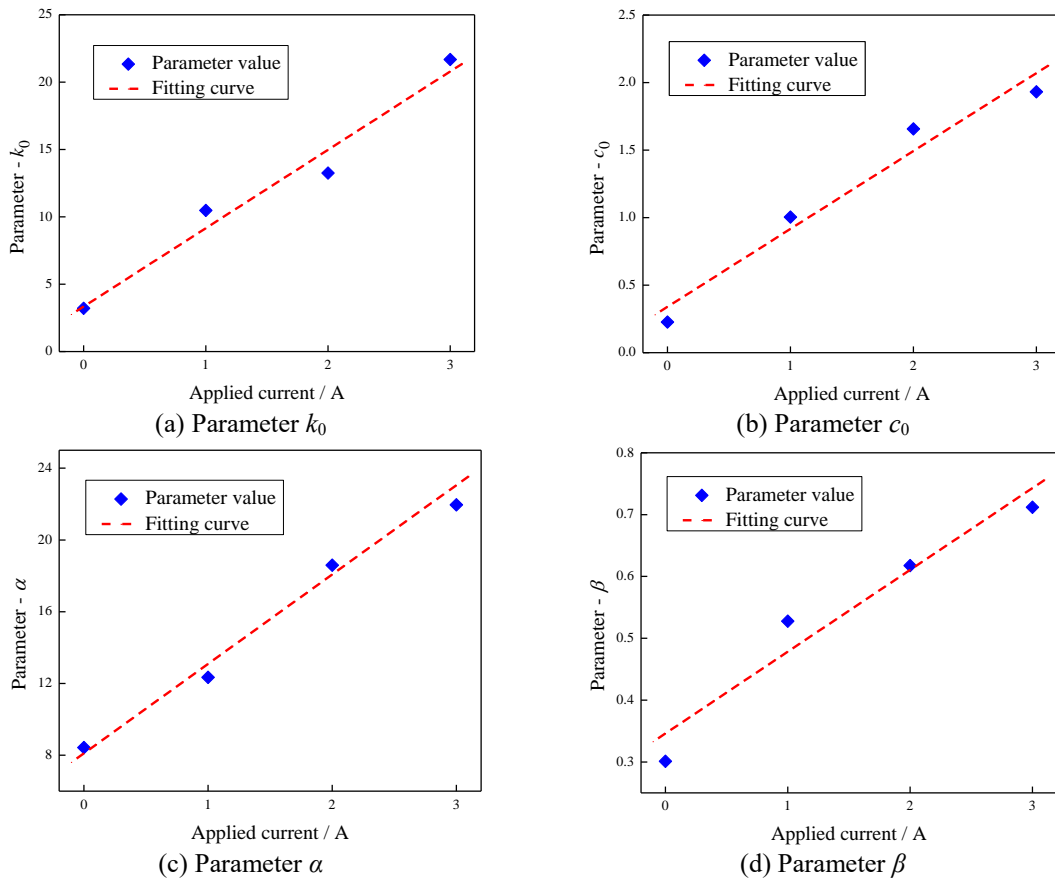


Fig. 12 Relationship between parameter values and applied current

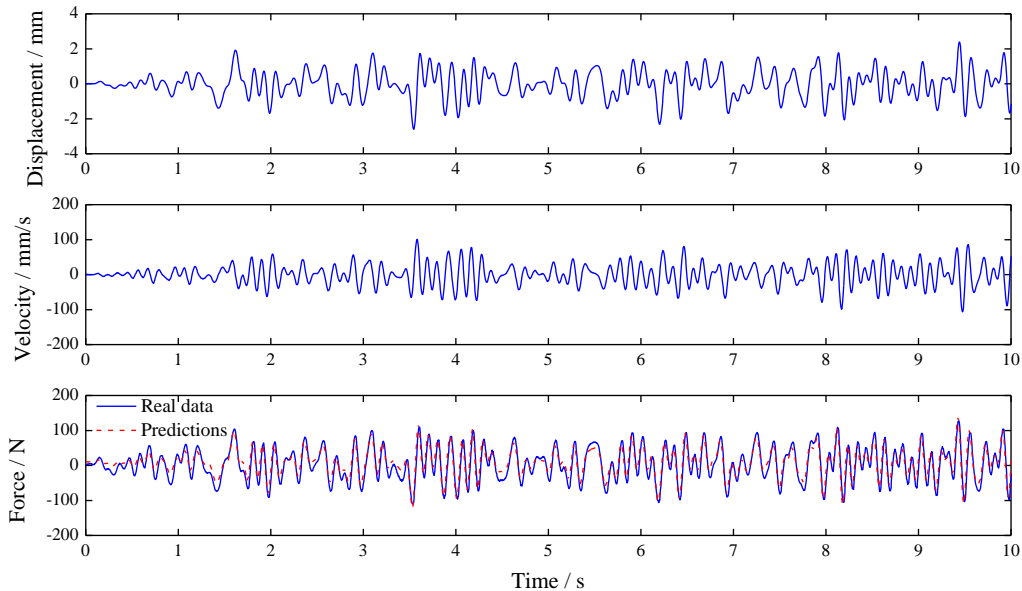


Fig. 13 Displacement, velocity and response comparison of MRE base isolator supplied with random excitation and 1A current level

Table 2 Expression coefficient values

Coefficient	Value
k_0^0	5.8161
k_0^1	3.3431
c_0^0	0.5767
c_0^1	0.3396
α^0	4.9810
α^1	8.1100
β^0	0.1322
β^1	0.3463

To evaluate the performance of this generalized field-dependent model, comparative loops are shown in Fig. 13, in which the measurements are obtained by loading device with the random excitation with maximal input amplitude of 4 mm and 1A applied current. The comparison results demonstrate that the nonlinear behaviour of the device is perfectly captured.

4. Application in vibration control of building structures

In this part, a controller based on the proposed field-dependent model is designed to realize the real-time adaptive control of building structures with MRE base isolators. A three-storey structure equipped with two smart devices subjected to four benchmark earthquake excitations is then used to validate the performance of the controller designed according to the proposed model.

4.1 System model of smart structure

The structural sketch of n -storey building model configured with two identified adaptively tuned MRE base isolators is shown in Fig. 14. Because the current-dependent MRE devices are rigidly installed underneath the base floor, the augmented building model is an $n+1$ degree-of-freedom (DOF) system. Assume the structural motion is sufficiently moderate that nonlinear effects may be neglected, then the floor motion equation can be written as

$$m_b \ddot{y}_b + c_b (\dot{y}_b - \dot{x}_g) - c_1 (\dot{y}_1 - \dot{y}_b) + k_b (y_b - x_g) - k_1 (y_1 - y_b) = f_b \tag{18}$$

where y_b is the absolute displacement of the base floor with respect to an inertial frame, x_g denotes the displacement of the ground that is induced by seismic-like ground acceleration \ddot{x}_g . Let $x_i = y_i - x_g$ ($i=b, 1, \dots, n$) describe the relative displacements between the ground and each mass, and contain the DOF of the system. Therefore, the motion equations of the structure can be written as

$$S_b : m_b \ddot{x}_b + (c_b + c_1) \dot{x}_b - c_1 \dot{x}_1 + (k_b + k_1) x_b - k_1 x_1 = f_b - m_b \ddot{x}_g \tag{19}$$

$$S_1 : m_1 \ddot{x}_1 - c_1 \dot{x}_b + (c_1 + c_2) \dot{x}_1 - c_2 \dot{x}_2 - k_1 x_b + (k_1 + k_2) x_1 - k_2 x_2 = -m_1 \ddot{x}_g \tag{20}$$

$$S_i : m_i \ddot{x}_i - c_i \dot{x}_{i-1} + (c_i + c_{i+1}) \dot{x}_i - c_{i+1} \dot{x}_{i+1} - k_i x_{i-1} + (k_i + k_{i+1}) x_i - k_{i+1} x_{i+1} = -m_i \ddot{x}_g \tag{21}$$

$$S_n : m_n \ddot{x}_n - c_n \dot{x}_{n-1} + c_n \dot{x}_n - k_n x_{n-1} + k_n x_n = -m_n \ddot{x}_g \tag{22}$$

The motion equations of the above system can be rewritten in the following matrix form

$$M\ddot{x} + C\dot{x} + Kx = \Gamma f_t - M\Theta\ddot{x}_g \tag{23}$$

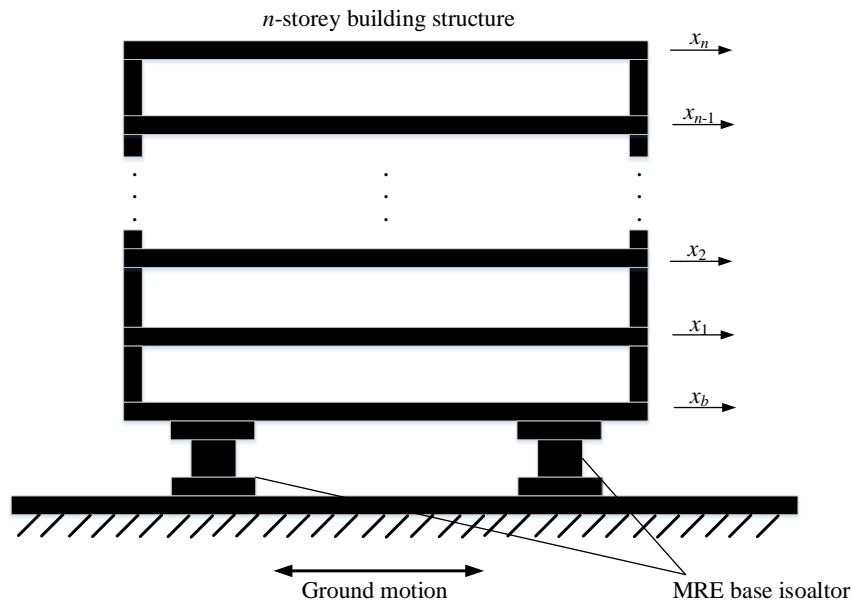


Fig. 14 Sketch of n -storey building structure

where $M = \text{diag}([m_i])$, $x = [x_i]^T \in \mathfrak{R}^{n+1}$, $i = b, 1, \dots, n$,

$$C = \begin{bmatrix} c_b + c_1 & -c_1 & 0 & \cdots & 0 & 0 & 0 \\ -c_1 & c_1 + c_2 & -c_2 & \cdots & 0 & 0 & 0 \\ \vdots & \vdots & \vdots & \vdots & \vdots & \vdots & \vdots \\ 0 & 0 & 0 & \cdots & -c_{n-1} & c_{n-1} + c_n & -c_n \\ 0 & 0 & 0 & \cdots & 0 & -c_n & c_n \end{bmatrix} \text{ and } K = \begin{bmatrix} k_b + k_1 & -k_1 & 0 & \cdots & 0 & 0 & 0 \\ -k_1 & k_1 + k_2 & -k_2 & \cdots & 0 & 0 & 0 \\ \vdots & \vdots & \vdots & \vdots & \vdots & \vdots & \vdots \\ 0 & 0 & 0 & \cdots & -k_{n-1} & k_{n-1} + k_n & -k_n \\ 0 & 0 & 0 & \cdots & 0 & -k_n & k_n \end{bmatrix}$$

The positive-definite matrices M , C and K represent the mass, damping and stiffness matrices of the system structure, respectively. f_i denotes the total control force exerted by the MRE base isolators. Γ denotes the position vector, which is determined by the placement of the MRE isolators in the structure. Θ denotes the column vector $[1 \dots 1]^T$. Because the mass matrix is non-singular, Eq. (23) can be rewritten as the state-space form

$$\dot{q} = Aq + b(q, i) + D \tag{24}$$

$$\begin{bmatrix} \dot{x} \\ \ddot{x} \end{bmatrix} = \begin{bmatrix} 0 & I \\ -M^{-1}\tilde{K} & -M^{-1}\tilde{C} \end{bmatrix} \begin{bmatrix} x \\ \dot{x} \end{bmatrix} + \begin{bmatrix} 0 \\ [-2m_b^{-1}(c_{E1}\dot{x}_b + k_{E1}x_b)i \quad 0 \quad \cdots \quad 0]^T \end{bmatrix} \tag{25}$$

$$+ \begin{bmatrix} 0 \\ [-2m_b^{-1}\alpha \sinh(\beta x_b) \quad 0 \quad \cdots \quad 0]^T \end{bmatrix} + \begin{bmatrix} 0 \\ \Theta \end{bmatrix} \ddot{x}_g$$

where $q = [x \ \dot{x}]^T$ is a state vector, $\mathbf{0}$ and \mathbf{I} denote the null matrix and identity matrix, respectively. A denotes the $2(n+1) \times 2(n+1)$ system matrix depending on the damping and stiffness of the structure while $b(q, i)$ is the non-affine function and D is the $2(n+1) \times 1$ disturbance matrix composed of model uncertainties D_1 and external excitation D_2 . Here, the first element of matrices \tilde{K} and \tilde{C} are $k_b + k_1 + 2k_{E0}$ and $c_b + c_1 + 2c_{E0}$, and all remaining elements are same as that in the matrices K and C . Therefore, the motion equations of an n -DOF smart building structure can be expressed as

$$\begin{bmatrix} \dot{x}_{(n+1) \times 1} \\ \ddot{x}_{(n+1) \times 1} \end{bmatrix} = \begin{bmatrix} 0_{(n+1) \times (n+1)} & I_{(n+1) \times (n+1)} \\ -M^{-1}\tilde{K} & -M^{-1}\tilde{C} \end{bmatrix} \begin{bmatrix} x \\ \dot{x} \end{bmatrix} + \begin{bmatrix} 0_{(n+1) \times 1} \\ [-2m_b^{-1}(c_{E1}\dot{x}_b + k_{E1}x_b)i \quad 0 \quad \cdots \quad 0]^T \end{bmatrix} \tag{26}$$

$$+ \begin{bmatrix} 0_{(n+1) \times 1} \\ [-2m_b^{-1}\alpha \sinh(\beta x_b) \quad 0 \quad \cdots \quad 0]^T \end{bmatrix} + \begin{bmatrix} 0_{(n+1) \times 1} \\ \Theta_{(n+1) \times 1} \end{bmatrix} \ddot{x}_g$$

where $M = \text{diag}([m_b \ m_1 \ \cdots \ m_n])$, $x = [x_b, x_1, \dots, x_n]^T \in \mathfrak{R}^{n+1}$

$$\tilde{C} = \begin{bmatrix} c_b + c_1 + 2c_{E0} & -c_1 & 0 & \cdots & 0 \\ -c_1 & c_1 + c_2 & -c_2 & \cdots & 0 \\ \vdots & \vdots & \vdots & \cdots & \vdots \\ 0 & 0 & 0 & \cdots & c_n \end{bmatrix} \text{ and } \tilde{K} = \begin{bmatrix} k_b + k_1 + 2k_{E0} & -k_1 & 0 & \cdots & 0 \\ -k_1 & k_1 + k_2 & -k_2 & \cdots & 0 \\ \vdots & \vdots & \vdots & \cdots & \vdots \\ 0 & 0 & 0 & \cdots & k_n \end{bmatrix}$$

4.2 Controller design based on proposed model

In this work, the second-order sliding mode (SOSM) control method is adopted in which the control action is applied to the second derivative of the sliding variable. The conventional sliding function can be defined as

$$s(t) = \dot{x}_b + \lambda x_b, \lambda > 0 \quad (27)$$

Here, the first and second derivatives of the sliding variable are considered, given as follows

$$\dot{s}(t) = \ddot{x}_b + \lambda \dot{x}_b \quad (28)$$

$$\ddot{s}(t) = \dddot{x}_b + \lambda \ddot{x}_b \quad (29)$$

Then, the base floor motion equation of the system can be rewritten as

$$m_b \ddot{x}_b + (c_b + c_1) \dot{x}_b - c_1 \dot{x}_1 + (k_b + k_1) x_b - k_1 x_1 = -2(c_{E0} + c_{E1} i) \dot{x}_b - 2(k_{E0} + k_{E1} i) x_b - 2(\alpha_0 + \alpha_1 i) \sinh[(\beta_0 + \beta_1 i) x_b] - m_b \ddot{x}_g \quad (30)$$

In this paper, the control signal is defined as the time rate of applied current variation to the base isolated building model. In this case, the derivative expression of Eq. (30) is obtained

$$\begin{aligned} m_b \ddot{x}_b = & -(c_b + c_1 + 2c_{E0}) \ddot{x}_b + c_1 \ddot{x}_1 - (k_b + k_1 + 2k_{E0}) \dot{x}_b + k_1 \dot{x}_1 \\ & - 2(c_{E1} \dot{x}_b + k_{E1} x_b) i - 2(\alpha_0 + \alpha_1 i) \cosh[(\beta_0 + \beta_1 i) x_b] (\beta_0 + \beta_1 i) \dot{x}_b a - m_b \ddot{x}_g \\ & - 2[c_{E1} \dot{x}_b + k_{E1} x_b + \alpha_1 \sinh[(\beta_0 + \beta_1 i) x_b] + (\alpha_0 + \alpha_1 i) \cosh[(\beta_0 + \beta_1 i) x_b] \beta_1 x_b] \frac{di}{dt} \end{aligned} \quad (31)$$

Hence, the second-order sliding variable is achieved

$$\ddot{s}(t) = \Phi(t, x_b, i) + \Psi(t, x_b, i) \frac{di}{dt} \quad (32)$$

where Φ and Ψ can be expressed by

$$\begin{aligned} \Phi(\cdot) = & -m_b^{-1} [(c_b + c_1 + 2c_{E0}) \ddot{x}_b - c_1 \ddot{x}_1 + (k_b + k_1 + 2k_{E0}) \dot{x}_b - k_1 \dot{x}_1 + 2(c_{E1} \dot{x}_b + k_{E1} x_b) i \\ & + 2(\alpha_0 + \alpha_1 i) \cosh[(\beta_0 + \beta_1 i) x_b] (\beta_0 + \beta_1 i) \dot{x}_b + \lambda \{(c_b + c_1 + 2c_{E0}) \dot{x}_b - c_1 \dot{x}_1 \\ & + (k_b + k_1 + 2k_{E0}) x_b - k_1 x_1 + 2(c_{E1} \dot{x}_b + k_{E1} x_b) i + 2\alpha \sinh(\beta x_b)\}] - \ddot{x}_g - \lambda \ddot{x}_g \end{aligned} \quad (33)$$

$$\Psi(\cdot) = -2m_b^{-1} [c_{E1} \dot{x}_b + k_{E1} x_b + \alpha_1 \sinh[(\beta_0 + \beta_1 i) x_b] + (\alpha_0 + \alpha_1 i) \cosh[(\beta_0 + \beta_1 i) x_b] \beta_1 x_b] \quad (34)$$

Here, by denoting $u = di/dt$ and $\nabla = \partial/\partial u$, the following standard expression will be acquired

$$\ddot{s}(t) = \Phi(t, x_b, i) + \Psi(t, x_b, i) u, \quad \Phi(\cdot) = \dot{s}|_{u=0}, \quad \Psi(\cdot) = \nabla \dot{s} \neq 0 \quad (35)$$

where Φ and Ψ meets the following global boundary condition with the concrete values of τ , v_m and v_M (Levant 2007, Pisano and Usai 2011)

$$\forall t > 0 \quad -\tau \leq \Phi(t, x_b, i) \leq \tau \quad \text{and} \quad 0 < v_m \leq \Psi(t, x_b, i) \leq v_M \quad (36)$$

This provides the following differential inclusion trajectories to zero for the finite-time convergence

$$\ddot{s}(t) \in [-\tau, \tau] + [v_m, v_M] u \quad (37)$$

Let $\eta_1 = s$ and $\eta_2 = \dot{s}$ describe the above equation in the matrix form

$$\dot{\eta}(t) \in G\eta(t) + h([- \tau, \tau] + [v_m, v_M]\phi(s, \dot{s})) \quad (38)$$

where $\eta = [s \ \dot{s}]^T$; G is the state matrix of the sliding variable and $G = \begin{bmatrix} 1 & 0 \\ 0 & 0 \end{bmatrix}$; h is the input matrix

where the control action is applied to the second derivative of the sliding variable and $h = \begin{bmatrix} 0 \\ 1 \end{bmatrix}$.

Then, the SOSM control, $u = di/dt = \phi(s, \dot{s})$, exists to steer the sliding function s and its time \dot{s} derivative to 0 asymptotically. Since the differential inclusions (37) and (38), understood in the Filippov sense (Filippov and Arscott 1988), are insensitive to the original system (Eq. (24)), such the controller is obviously robust with respect to any perturbations preserving (Levant 2007, Pisano and Usai 2011).

The actual current command to the MRE base isolator is bounded within the range of $0 \leq i \leq i_M$. According to (Ha *et al.* 2013), the control current $k(t)$ can be achieved by integrating the feedback control signal $u(t)$. Here, a quasi-continuous controller is adopted, given as follows

$$u(t) = \begin{cases} u_1 & \text{if } s \neq 0 \text{ and } \kappa(t) \leq i_M \\ u_2 & \text{if } s = 0 \text{ and } \kappa(t) \leq i_M \\ 0 & \text{if } \kappa(t) > i_M \end{cases} \quad (39)$$

where $u_1 = \min[\rho, \max\{-\rho, -\zeta(\dot{s}|s|^{-0.5} + \vartheta \text{sign}(s))\}]$, $u_2 = -\rho \text{sign}(\dot{s})$. ρ , ζ and ϑ are positive constants, and meet the relationships of $\rho v_m - \tau > 0.5\vartheta^2$ and $\zeta \vartheta > \rho$. The control law (39) allows increasing the value of ζ to get closer to the parabola $\dot{s} + |s|^{0.5} \vartheta \text{sign}(s) = 0$ without adding the control magnitude.

4.3 Case study

To evaluate the performance of the designed controller based on the proposed model, a numerical study is undertaken according to the seismic response mitigation of building structure. In this study, a three-storey benchmark building model, developed by Dyke *et al.* (1996), is used to make up the smart structure together with two MRE base isolators. The parameter values of building model were identified by Dyke *et al.*, shown in Table 3. The mechanical properties of MRE base isolator can be found from Eqs. (13)-(17) and Table 2. To verify the effect of the designed controller on seismic response mitigation, four benchmark earthquakes are also employed to excite the smart structure, i.e. EI-Centro 1940, Hachinohe 1968, Northridge 1994 and Kobe 1995. Among four earthquake excitations, the former two are representatives of far field earthquakes with medium ground movements while the latter two are near field, more grievous earthquake events. To make sure the fundamental frequency of smart structure with the main seismic frequency spectrum, four benchmark earthquake records are scaled down by 0.5. Accordingly, the passive structure responses would be greatly reinforcement so that the performance of the proposed method would be better verified.

Fig. 15 records time-history control signal changes of MRE base isolators during the seismic

excitations. It is apparent that all the applied currents continuously vary between 0A and 2.5A, which meets the maximum current limitation requirement (3A). It is chiefly because the coils in the isolator will generate a massive source of heat when the isolator is supplied with varied currents, leading to unstable performance of the device.

Floor acceleration is one of the most important responses to represent the effectiveness of earthquake proof of the proposed smart isolation system. Generally, the floor acceleration ascends with the increasing of building level due to the first-mode of the structure subjected to the seismic excitations. As a result, the floor acceleration continuously ascends with the increase of structure level, which means that the maximum acceleration always happens at the top level of the structure.

Table 3 Property values of three-storey building model

Floor No.	Mass (kg)	Stiffness (kN/m)	Damping (N·s/m)
1	98.3	516	125
2	98.3	684	50
3	98.3	684	50

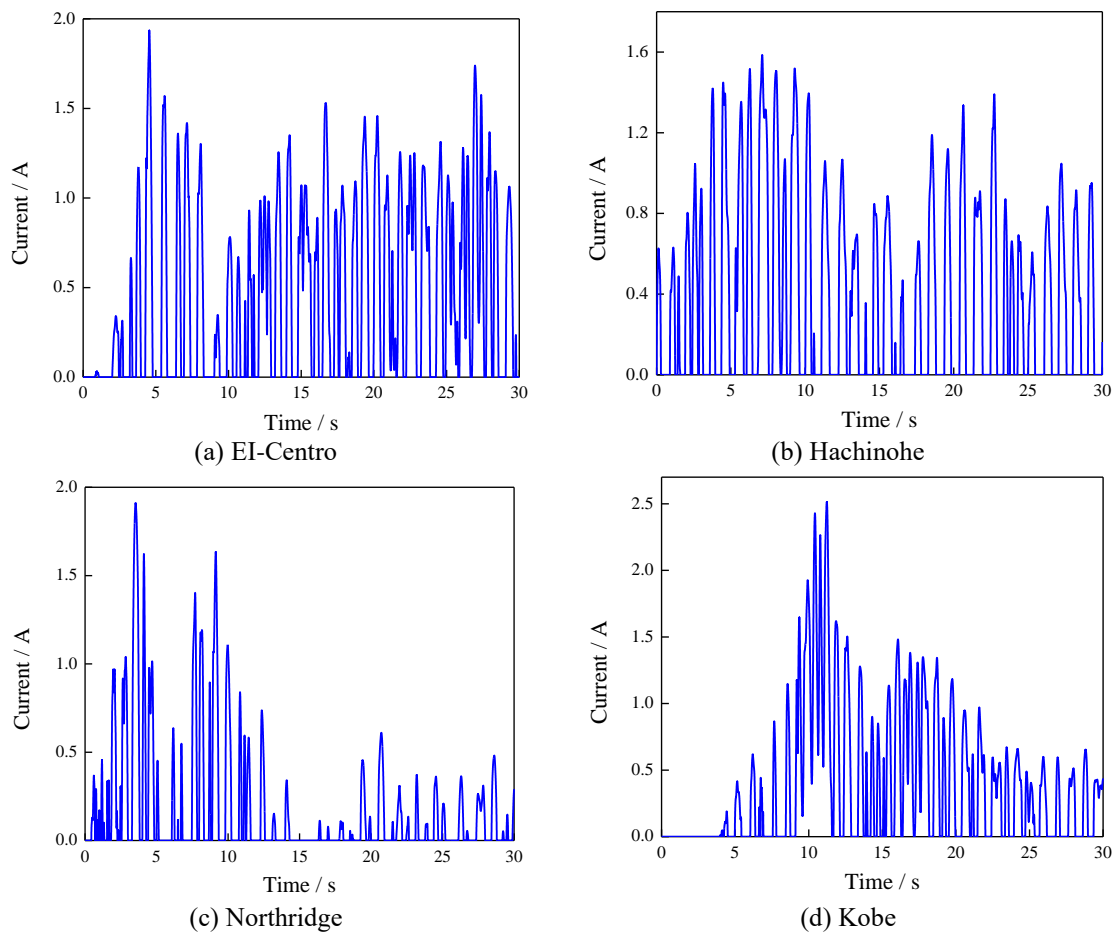


Fig. 15 Applied current control signals

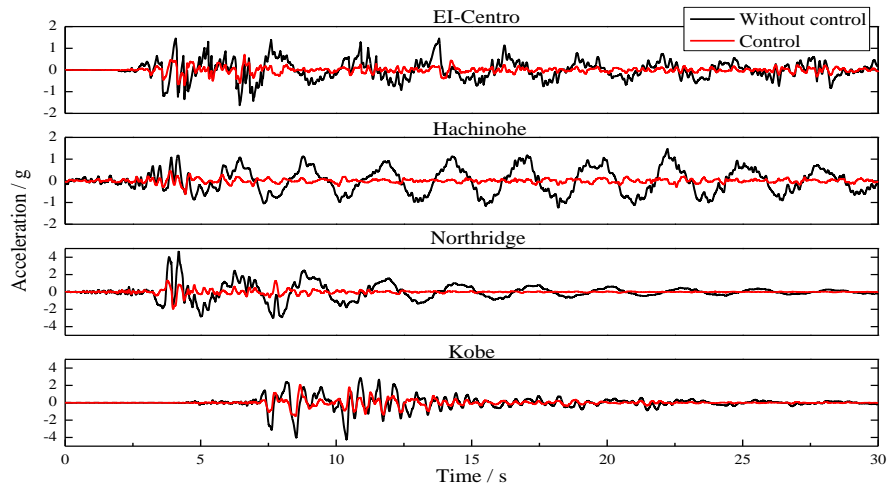


Fig. 16 Response comparisons between passive and controlled structures under four earthquake excitations

Hence, the acceleration change when the acceleration of the third floor arrives at its peak value is employed as the evaluation index to assess the intensity of the vibration and deformation of the building. Fig. 16 shows the time-series top floor acceleration comparison of smart structure with and without the proposed model-based control strategy under four benchmark seismic excitations. The black dot lines denote the responses of smart structure without control while the red solid line illustrates the responses of smart building with the controller based on the proposed model. From the results in figure, it is clearly seen that with the semi-active control strategy based on the proposed model, the structure is able to remarkably reduce the acceleration responses for all the seismic cases. Especially for EI-Centro and Hachinohe earthquakes, the smart structure with the controller is shown more useful than passive structure in restraining the structure vibration.

Apart from the time historical acceleration at the top floor, both inter-storey drift and peak acceleration of all the floors are also significant indices in describing the effectiveness of the controller based on the proposed model. Floor peak acceleration is capable of providing a rough structure configuration with most serious vibration while the inter-storey drift at each floor represents the deformation degree between two neighbouring levels. Fig. 17 compares both inter-storey drift and peak acceleration of all the floors between passive and controlled smart structure under four earthquake excitations. It is obvious that the floor peak acceleration always rise with the structure height while the inter-storey drift shows the dropping relationship with the floor for all the cases of earthquakes, which accords with previous analysis. Another noteworthy result is that compared with passive structure, the controlled one changes relatively less in terms of two indices at all floors. These comparisons sufficiently prove that the MRE base isolator together with semi-active control based on proposed model has a promising application prospect in protection and vibration mitigation of building structure.

5. Conclusions

This work first presents a new hysteresis model to characterize the adaptively tuned MRE base

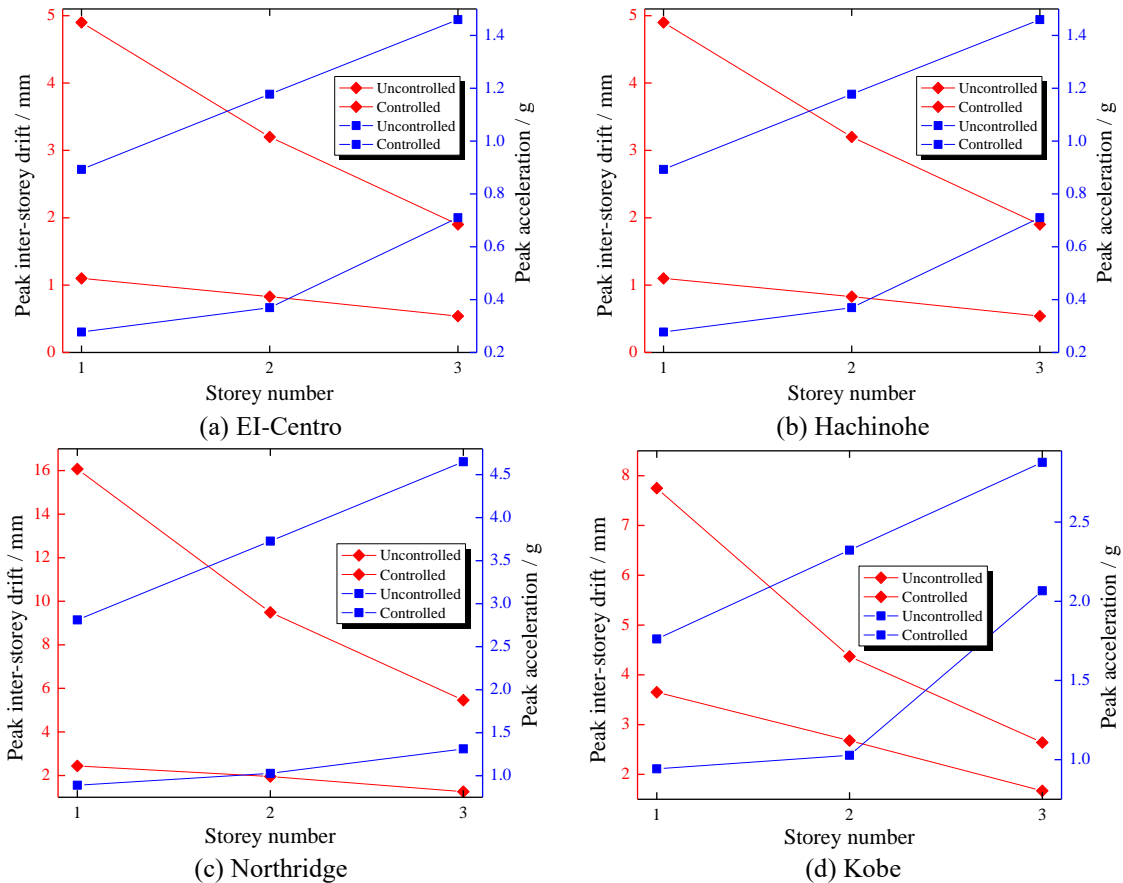


Fig. 17 Comparisons of inter-storey drift and peak acceleration at each floor between passive and control structures under four earthquake excitations

isolator, which is developed for seismic mitigation of building structures via semi-active control. This newly designed model is constituted by a nonlinear spring and a Voigt component connected in a parallel way with the benefits of fewer parameters and simple expression without any differential equations, compared with classical Bouc-Wen model. Then, based on the experimental data, the model parameters are identified using FFOA, which are able to be summarized as the functions of applied current. Finally, a second-order sliding mode controller, based on this field-dependent model, is proposed to implement semi-active control of MRE isolator. To evaluate its effectiveness, a numerical study is conducted using a three-storey benchmark building model as well as four commonly used seismic excitations. The analysis results show that the controlled smart structure using the proposed method outperforms the passive structure in terms of floor acceleration and inter-storey drift.

Acknowledgements

This work was supported by Australian Research Council through Discovery Project (Grant

No. DP150102636) as well as Blue Sky Research Fund from Faculty of Engineering and IT, University of Technology Sydney (UTS). In addition, the authors are particularly grateful to the staff of UTS structure lab for their help in the experimental testing.

References

- Agrawal, A.K. and Yang, J.N. (1999), "Design of passive energy dissipation systems based on LQR control methods", *J. Int. Mat. Syst. Struct.*, **10**(12), 933-944.
- Behrooz, M., Wang, X. and Gordaniejad, F. (2014a), "Modeling of a new semi-active/passive magnetorheological elastomer isolator", *Smart Mater. Struct.*, **23**(4), 045013.
- Behrooz, M., Wang, X. and Gordaniejad, F. (2014b), "Performance of a new semi-active/passive magnetorheological elastomer isoaltor", *Smart Mater. Struct.*, **23**(4), 045014.
- Chen, L. and Jerrams, S. (2011), "A rheological model of the dynamic behaviour of magnetorheological elastomers", *J. Appl. Phys.*, **110**(1), 013513.
- Du, H., Li, W. and Zhang, N. (2011), "Semi-active variable stiffness vibration control of vehicle seat suspension using an MR elastomer isolator", *Smart Mater. Struct.*, **20**(10), 105003.
- Dyke, S.J., Spencer, B.F., Sain, M.K. and Carlson, J.D. (1996), "Modeling and control of magnetorheological dampers for seismic response reduction", *Smart Mater. Struct.*, **5**(5), 565-575.
- Eem, S., Jung, H. and Koo, J. (2012), "Modeling of magneto-rheological elastomers for harmonic shear deformation", *IEEE Trans. Magnet.*, **48**(11), 3080-3083.
- Feng, J., Xuan, S., Liu, T., Ge, L., Yan, L., Zhou, H. and Gong, X. (2015), "The prestress-dependent mechanical response of magnetorheological elastomers", *Smart Mater. Struct.*, **24**(8), 085032.
- Filippov, A.F. and Arscott, F.M. (1988), *Differential equations with discontinuous righthand sides*, Kluwer Academic Publishers, Netherlands.
- Ginder, J.M., Nichols, M.E., Elie, L.D. and Tardiff, J.L. (1999), "Magnetorheological elastomers: properties and applications", *Proc. SPIE*, 3675, 131-138.
- Gu, X., Li, J., Li, Y. and Askari, M. (2015), "Frequency control of smart base isolation system employing a novel adaptive magnetorheological elastomer base isolator", *J. Int. Mat. Syst. Struct.*, **27**(7), 849-858.
- Ha, Q.P., Kwok, N.M., Nguyen, M.T., Li, J. and Samali, B. (2008), "Mitigation of seismic responses of building structures using MR dampers with Lyapunov-based control", *Struct. Control Hlth.*, **15**(6), 604-621.
- Ha, Q.P., Nguyen, M.T., Li, J. and Kwok, N.M. (2013), "Smart structures with current-driven MR dampers: modelling and second-order sliding mode control", *IEEE-ASME Trans. Mech.*, **18**(6), 1702-1711.
- Ha, Q.P., Royel, S., Li, J. and Li, Y. (2015), "Hysteresis modeling of smart structure MR devices using describing functions", *IEEE-ASME Trans. Mech.*, **21**(1), 44-50.
- Hosseini, M. and Farsangi, E.N. (2012), "Telescopic columns as a new base isolation system for vibration control of high-rise buildings", *Earthq. Struct.*, **3**(6), 853-867.
- Jansen, L. and Dyke, S. (2000), "Semiactive control strategies for MR dampers: comparative study", *J. Eng. Mech.*, **126**(8), 795-803.
- Levant, A. (2007), "Principles of 2-sliding mode design", *Automatica*, **43**(4), 576-586.
- Li, W.H., Zhou, Y. and Tian, T.F. (2010), "Viscoelastic properties of MR elastomers under harmonic loading", *Rheol Acta*, **49**(7), 733-740.
- Li, Y. and Li, J. (2015), "A highly adjustable base isolator utilizing magnetorheological elastomer: experimental testing and modeling", *J. Vib. Acoust.*, **137**(1), 011009.
- Li, Y., Li, J., Li, W. and Du, H. (2014), "A state-of-the-art review on magnetorheological elastomer devices", *Smart Mater. Struct.*, **23**(12), 123001.
- Li, Y., Li, J., Tian, T. and Li, W. (2013), "A highly adjustable magnetorheological elastomer base isolator for applications of real-time adaptive control", *Smart Mater. Struct.*, **22**(9), 095020.
- Mei, Z., Peng, Y. and Li, J. (2013), "Experimental and analytical studies on stochastic seismic response

- control of structures with MR dampers”, *Earthq. Struct.*, **5**(4), 395-416.
- Murase, M. and Tsuji, M. and Takewaki, I. (2013), “Smart passive control of buildings with higher redundancy and robustness using base-isolation and inter-connection”, *Earthq. Struct.*, **4**(6), 649-670.
- Pan, W.T. (2012), “A new fruit fly optimization algorithm: taking the financial distress model as an example”, *Knowl-based Syst.*, **26**(2), 69-74.
- Pan, W.T. (2013), “Using modified fruit fly optimization algorithm to perform the function test and case studies”, *Connect. Sci.*, **25**(2-3), 151-160.
- Pan, W.T. (2014), “Mixed modified fruit fly optimization algorithm with general regression neural network to build oil and gold prices forecasting model”, *Kybernetes*, **43**(7), 1053-1063.
- Pisano, A. and Usai, E. (2011), “Sliding mode control: A survey with applications in math”, *Math. Comput. Simulat.*, **81**(5), 954-979.
- Spencer, B.F. (2004), “Benchmark structural control problems for seismic and wind-excited structures: Editorial”, *J. Eng. Mech.*, **130**(4), 363-365.
- Spencer, B.F. and Nagarajaiah, S. (2003), “State of the art of structural control”, *J. Struct. Eng.*, **129**(7), 845-856.
- Takewaki, I. and Tsujimoto, H. (2011), “Scaling of design earthquake ground motions for tall buildings based on drift and input energy demands”, *Earthq. Struct.*, **2**(2), 171-187.
- Tavakoli, H.R., Naghavi, F. and Goltabar, A.R. (2015), “Effect of base isolation systems on increasing the resistance of structures subjected to progressive collapse”, *Earthq. Struct.*, **9**(3), 639-656.
- Yang, J., Du, H., Li, W., Li, Y., Li, J., Sun, S. and Deng, H.X. (2013), “Experimental study and modeling of a novel magnetorheological elastomer isolator”, *Smart Mater. Struct.*, **22**(11), 117001.
- Yang, J., Sun, S.S., Du, H., Li, W.H., Alici, G. and Deng, H.X. (2014), “A novel magnetorheological elastomer isolator with negative changing stiffness for vibration reduction”, *Smart Mater. Struct.*, **23**(10), 105023.
- Yu, Y., Li, Y. and Li, J. (2015a), “Forecasting hysteresis behaviours of magnetorheological elastomer base isolator utilizing a hybrid model based on support vector regression and improved particle swarm optimization”, *Smart Mater. Struct.*, **24**(3), 035025.
- Yu, Y., Li, Y. and Li, J. (2015b), “Parameter identification and sensitivity analysis of an improved LuGre friction model for magnetorheological elastomer base isolator”, *Meccanica*, **50**(11): 2691-2707.
- Yu, Y., Li, Y., Li, J. and Gu, X. (2016), “A hysteresis model for dynamic behaviour of magnetorheological elastomer base isolator”, *Smart Mater. Struct.*, **25**(5), 055029.